

# Planar Sheets Meet Negative Curvature Liquid Interfaces

Zhenwei Yao,\* Mark Bowick,† Xu Ma, and Rastko Sknepnek

*Department of Physics, Syracuse University, Syracuse, New York 13244-1130, USA*

If an inextensible thin sheet is adhered to a substrate with a negative Gaussian curvature it will experience stress due to geometric frustration. We analyze the consequences of such geometric frustration using analytic arguments and numerical simulations. Both concentric wrinkles and eye-like folds are shown to be compatible with negative curvatures. Which pattern will be realized depends on the curvature of the substrate. We discuss both types of folding patterns and determine the phase diagram governing their appearance.

Geometric frustration occurs in wrapping a spherical Mozartkugel (“Mozart sphere”) with planar foil [1–3]. The extra circumference at the edge of the planar sheet compared to the spherical substrate to which it is conforming gives rise to ridges, narrow deformed regions that occupy a small fraction of the total available volume and along which the energy is focused [4]. Recently the frustration of a thin circular elastic sheet of  $\approx 1\text{mm}$  size covering the cap of a spherical droplet has been studied [5]. At first fine radial wrinkles appear at the edge of the sheet and then become unstable to localized folds as the size of the droplet decreases. One expects the situation to be quite different for a sheet conforming to a negative curvatures surface – in this case the edge of the sheet is stretched tangentially as opposed to being compressed on spherical geometry. A completely different frustration pattern on the planar sheet is thus expected. In this paper, we study the wrinkle/fold structure in an elasto-capillary system on a flat sheet conforming to a negatively curved substrate.

The system we treat has two parts: an inextensible thin elastic hydrophilic sheet and a saddle-like fluid interface with negative curvature. The size of the elastic sheet is taken to be much bigger than the elasto-capillary length  $\sqrt{\kappa/\sigma}$ , so that surface tension  $\sigma$  dominates over the bending rigidity  $\kappa$  [6]. Note that a standard sheet of paper can be regarded as inextensible and be used to demonstrate the bending of a thin elastic sheet [7]. When such an inextensible elastic sheet is placed on a negative curvature liquid interface the capillary force pulls the planar sheet into full contact with the liquid interface.

Complete contact between a planar sheet and a curved fluid substrate by capillary forces introduces a wrinkle/fold pattern, which redefines the metric of the planar sheet according to the curvature of the background geometry. The modification of the metric leads to the change of shape. This concept has been utilized to design responsive buckled surfaces [10]. The curved surface endows its metric to the flat sheet via their full contact. The inherited metric on the flat sheet as well as its elasticity determines the wrinkle/fold structure. Which wrinkle/fold patterns are compatible with negative curvatures? The art of origami provides some inspiration. It is shown in origami that regular concentric or square wrinkles with alternating peaks and valleys on a piece of paper can induce a negative curvature, as demonstrated

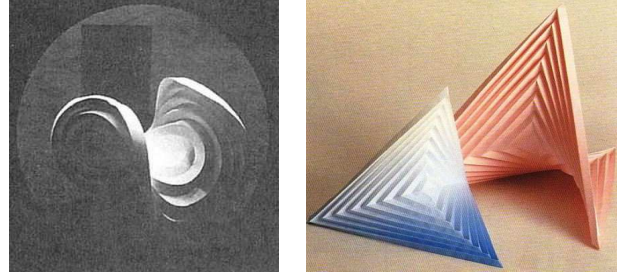


FIG. 1. (color online) Wrinkles of alternating peaks and valleys on a piece of paper redefine the metric, automatically bringing the flat paper to a saddle-like shape. It is shown in the text that the effect of concentric wrinkles is equivalent to inserting a wedge of some angle in the sense of redefining the metric. (a) is excerpted from Ref. [8], and (b) is from Ref. [9] where the method to make it is described in detail.

in Fig. 1.

In what follows we will prove that the effect of concentric wrinkles is equivalent to inserting an angular wedge in the sense of redefining the metric. The wavelength and amplitude of the concentric wrinkles determine the angle of the wedge. The wrinkled sheet is parameterized as  $\vec{x}(r, \theta) = \{r \cos \theta, r \sin \theta, a_k \cos(kr)\}$ , where  $a_k$  is the amplitude of the wrinkles and  $k$  is the wavenumber  $k = 2\pi/\lambda$ . The nonzero components of the metric tensor are  $g_{11} = 1 + x^2 \sin^2(kr)$  and  $g_{22} = r^2$ , where  $x = a_k k$ . The imposed wrinkles transform the original wrinkled shell into a new surface denoted by  $\Sigma$  that we take coincident with the curved substrate. On this new surface the metric is redefined such that the geodesic distance (denoted as  $r$ ) from the center of the disk to the first peak is  $r_0 = \lambda$ . The corresponding real distance on the original sheet is  $l_0 = \int_0^\lambda \sqrt{g_{11}} dr = \frac{1}{k} E(x)$ , where  $E(x) = \int_0^{2\pi} dy \sqrt{1 + x^2 \sin^2 y}$ . As  $a_k \rightarrow 0$ ,  $l_0 \rightarrow \lambda$ , as expected. Due to the inextensibility of the paper model, the mapping from the originally flat sheet to a wrinkled shape is isometric and thus length-preserving. The perimeter of the circle with radius  $r$  in the new surface  $\Sigma$  is thus  $C(r) = 2\pi l(r) \equiv 2\pi r + r\alpha$ , where  $l(r) = l_0 kr / (2\pi)$ . Here  $\alpha$  is interpreted as the angle of the inserted wedge:

$$\alpha = 2\pi \left( \frac{l_0}{\lambda} - 1 \right) > 0. \quad (1)$$

The positive sign of  $\alpha$  indicates that concentric wrinkles

are equivalent to *inserting* a wedge in redefining the metric. The inserted wedge buckles a flat disk to a saddle-like shape with negative curvature in three-dimensional Euclidean space [11], as do concentric wrinkles. These two ways of introducing negative curvature - either inserting material or imposing concentric wrinkles - are related via the expression for  $C(r)$ . The first method changes the perimeter without changing the radius, while it is the opposite for the second method. By expanding the expression for  $l_0$  in terms of small  $x$ , one finds  $C(r) = 2\pi r + \frac{\pi}{3}k^2x^2r^3 + \mathcal{O}(x)$ . By inserting this into  $K_G = \lim_{r \rightarrow 0} 3[2\pi r - C(r)]/(\pi r^3)$  [12], the curvature at the center of the surface  $\Sigma$  is found to be

$$K_G = -a_k^2 k^4. \quad (2)$$

Eq. (2) shows that increasing the amplitude or the frequency of the concentric wrinkles results in greater curvature of the surface, with greater sensitivity to the frequency. The curvature of the background geometry determines the amplitude and wavelength of the concentric wrinkles according to the product  $a_k^2 k^4$ .

It is worth mentioning that by increasing (“growing”) the radius of a flat disk while keeping the perimeter invariant, we get a positive curvature surface, which may buckle to various patterns depending on its elasticity. This elasticity paradigm has been used to explain the phyllotactic patterns of Fibonacci-like sequences on plants [13]. Wrinkles of concentric squares can buckle a square piece of paper to a beautiful hyperbolic parabola with negative curvature as shown in Fig. 1(b). Prescribed metrics via the design of wrinkles can even transform a flat piece of paper into a rich variety of structures, including the DNA double helix [14].

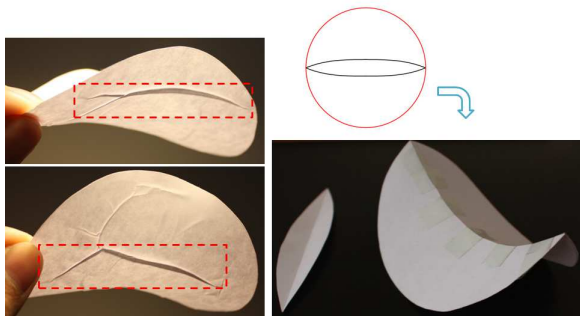


FIG. 2. (color online) A branch-like fold pattern appears on a flat paper disk by wrapping it on a negative curvature surface (left figures). The folds in the red rectangles are equivalent to removing eye-like areas as shown in the upper right figure. The buckled shape (the lower right figure; the leaf-like object therein is the removed material) of a flat disk due to an isolated fold is obtained by “closing the eye”.

In addition to wrinkles, localized folds can also change the metric [15]. By attaching a paper disk to a negative curvature surface one finds typical branch-like fold patterns as shown in Fig. 2 (the left two photos are the same

deformed paper disk from different perspectives). A light beam directly illuminates the paper disk from above, so the folds are seen clearly as black curves. The folds on the sheet can be roughly classified as principal ones (in red rectangles) and fine ones (barely seen above the red rectangle in the left lower figure). Their role in “screening” curvature is similar to topological defects in crystalline order on a curved surface [16]. The feature of the observed folds is that the amount of the folded material decreases towards their ends. Similar folds are also found in the interior side of a bent tube where the curvature is negative [17]. We analyze an isolated fold to illustrate that it is compatible with negative curvature geometry, which is analogous to the compatibility of a seven-fold disclination with negative curvature geometry. The effect of such folds is to remove an eye-like area from a flat disk. The buckled shape (see the lower right figure in Fig. 2) due to the fold, or equivalently the removal of an eye-like area, is obtained by “closing the eye”. The curvature of the buckled shape is negative; the disk curves up along the fold and curves down along the orthogonal direction. The removal of an eye-like area is equivalent to inserting a wedge, because more material is removed at the center than on the edge. The profile of the eye-like fold can be determined by the curvature of the background geometry. The perimeter of a circle with geodesic radius  $r$  on a disk with an eye-like area removed is estimated as  $C(r) \approx 2\pi r + 4(h(0) - h(r))$ , where  $2h(r)$  is the width of a fold. For a small-sized fold (in comparison with  $\sqrt{1/|K_G|}$ ), one finds  $h(r) = h(0) + \frac{\pi}{12}K_G r^3$  by inserting  $C(r)$  into the expression for the Gaussian curvature. From  $h(r = L/2) = 0$ , we see that the length of the fold is controlled by the curvature according to  $L = 2 \left( \frac{12h(0)}{\pi|K_G|} \right)^{1/3}$ . In contrast, it is interesting to note that reversed eye-like folds are found in one’s palms. It seems that the two main lines - head line and heart line following the terminology of palmistry - are compatible with positive curvatures as the width of these lines increases from the center to the edge of a palm.

We now examine the transition between wrinkle and fold patterns. In the regime of large surface tension, the ground state of an elasto-capillary system is dominated by the surface energy difference before and after a planar sheet is attached to the liquid interface:  $\Delta F = \sigma_{LA}A_{sheet} + \sigma_{LS}A_{coverage} - \sigma_{LA}A_{substrate} = -\sigma_{LS}A_{coverage} + \text{const.}$   $\sigma_{IJ}$  is the surface tension between phases  $I$  and  $J$  with  $L$ ,  $A$ , and  $S$  standing for liquid, air, and elastic sheet, respectively.  $A_{coverage}$  is the area of the liquid substrate occupied by the elastic sheet, which is smaller than the area of the sheet  $A_{sheet}$  due to its deformation.  $A_{substrate}$  is the sum of the occupied and unoccupied substrate areas, which is a constant. The surface energy turns out to depend only on  $A_{coverage}$ ; the larger it is, the smaller the energy is. Unlike a planar sheet on a positive curvature surface, the deformation at the edge of a planar sheet on a negative curvature surface may be ignored. Therefore, the optimal contour shape of

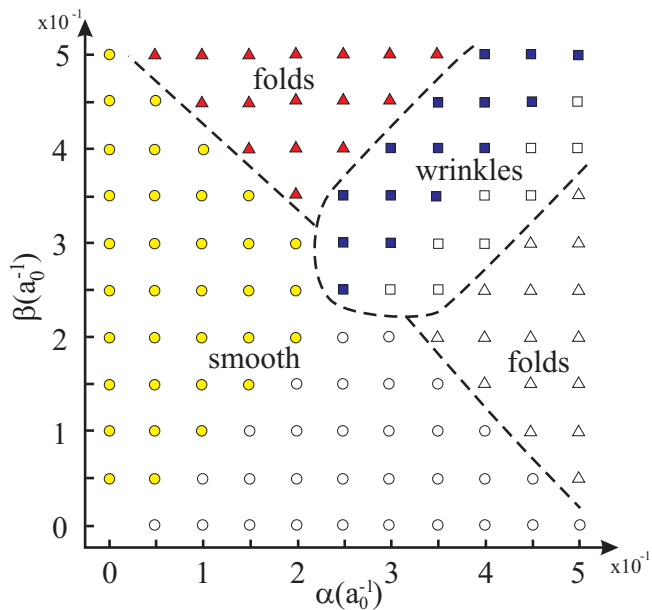


FIG. 3. (color online) The phase diagram of a deformed sheet on a negative curvature surface,  $z(x, y) = \alpha x^2 - \beta y^2$ . Wrinkles (squares) on the sheet occur near the isotropic region ( $\alpha/\beta \approx 1$ ) while folds (triangles) are found in the highly anisotropic regions ( $\alpha/\beta$  far from unity). For very small  $\alpha$  and  $\beta$  the sheet is compliant with the adhering surface. This region is designated as smooth (circles). Filled symbols indicate parameters for which simulations were performed. The phase diagram is symmetric with respect to the  $\alpha = \beta$  line. Mirror images of the simulated points are represented as open symbols.

a deformed sheet on the liquid substrate is the one that maximizes the coverage area while keeping the perimeter fixed. This is exactly the classical isoperimetric problem, in this case on a negative curvature surface. For constant curvature surfaces, the classical isoperimetric solution in the Euclidean plane is also valid with the circle in  $\mathbb{E}^2$  being replaced by a geodesic circle [18]. On a general surface with varying negative curvature, there is no exact mathematical result available. The physical picture, however, is rather interesting: a deformed sheet fully attached to a curved liquid substrate will migrate to the region where it can extend as far as possible to maximize the contact area; the driving forces are the capillary force and the release of the bending energy in this curvature-driven migration process.

In order to further explore the deformation patterns we have performed numerical simulations of a thin elastic sheet adhered to a substrate with negative curvature. For an isotropic material the stretching and bending energies are given as [19]

$$E_s = \frac{t}{2} \int dA \frac{E}{1+\nu} \left( \frac{\nu}{1-\nu} u_\alpha^\alpha u_\beta^\beta + u_\alpha^\beta u_\beta^\alpha \right), \quad (3)$$

$$E_b = \frac{t^3}{24} \int dA \frac{E}{1+\nu} \left( \frac{\nu}{1-\nu} b_\alpha^\alpha b_\beta^\beta + b_\alpha^\beta b_\beta^\alpha \right). \quad (4)$$

Here  $\alpha, \beta \in \{x, y\}$ ,  $E$  is the three-dimensional Young's modulus and  $Y = Et$  with  $t$  being the sheet thickness;  $u_{\alpha\beta} = \frac{1}{2}(g_{\alpha\beta} - \bar{g}_{\alpha\beta})$  is the strain tensor with  $\bar{g}_{\alpha\beta}(g_{\alpha\beta})$  being the metric tensor of the reference (deformed) state. The reference metric is assumed to be flat, i.e.,  $\bar{g}_{\alpha\beta} = \delta_{\alpha\beta}$ .  $b_{\alpha\beta}$  is the second fundamental form [20],  $dA = \sqrt{|\bar{g}|} dx dy$  is the area element and  $\nu$  is the Poisson's ratio. Finally,  $u_\alpha^\beta = \bar{g}^{\beta\gamma} u_{\alpha\gamma}$  and  $b_\alpha^\beta = \bar{g}^{\beta\gamma} b_{\alpha\gamma}$ . With the mean curvature  $H \equiv \frac{1}{2} b_\alpha^\alpha$  and the Gaussian curvature  $K_G \equiv \det(b_\alpha^\beta)$ ,  $E_b = \int dA \kappa (2H^2 - (1-\nu)K_G)$ , where the bending rigidity is  $\kappa = \frac{t^3}{12} \frac{E}{(1-\nu^2)}$ . Since the deformations of the sheet do not change its topology, the Gauss-Bonnet theorem [20] ensures that  $\int dA K_G$  is constant and the Gaussian curvature term can be omitted.

We find the relaxed shapes of the sheet by performing simulated annealing Monte Carlo (MC) simulations of a discrete triangular mesh. The discrete form of the stretching energy Eq. (3) is [21, 22]

$$E_s^{dis.} = \frac{Y}{8(1+\nu)} \sum_T \left( \frac{\nu}{1-\nu} (\text{Tr} \hat{F})^2 + \text{Tr} \hat{F}^2 \right) A_T, \quad (5)$$

where  $\hat{F} = \hat{g}^{-1} \hat{g} - \hat{I}$ ,  $A_T$  is a mesh triangle area, and the sum is carried out over all triangles.  $\hat{g}$  and  $\hat{g}$  are the discrete counterparts of the reference and actual metric tensors, respectively, whose elements are the scalar products of the two vectors spanning each triangle before and after the deformation. By assuming that the sheet has no spontaneous curvature, the bending energy (Eq. (4)) of the discrete mesh is [23, 24]

$$E_b^{dis.} = 2\kappa \sum_i \left( \frac{(\nabla_{\mathbf{r}_i} A_i) \cdot \mathbf{N}_i}{\mathbf{N}_i \cdot \mathbf{N}_i} \right)^2 A_i, \quad (6)$$

where  $\nabla_{\mathbf{r}_i}$  is the gradient with respect to the position of vertex  $i$  and the sum is over all vertices.  $A_i = \frac{1}{3} \sum_{T \in \Omega_i} A_T$  is the vertex area, with  $\Omega_i$  being the vertex "star", i.e. the set of all triangles that share vertex  $i$ .  $A_T = \frac{1}{2} |(\mathbf{r}_j^{(T)} - \mathbf{r}_i) \times (\mathbf{r}_k^{(T)} - \mathbf{r}_i)|$ , where  $\mathbf{r}_i$ ,  $\mathbf{r}_j^{(T)}$  and  $\mathbf{r}_k^{(T)}$  are the coordinate vectors of the vertices of  $T$ . We omitted  $(T)$  in the superscript of vector  $\mathbf{r}_i$  since it is shared by all  $T \in \Omega_i$ .  $\mathbf{N}_i = \nabla_{\mathbf{r}_i} V_i$  is a volume gradient, with the volume [25]  $V_i = \frac{1}{6} |\mathbf{r}_i \cdot \sum_T (\mathbf{r}_j^{(T)} \times \mathbf{r}_k^{(T)})|$ . The sheet is assumed to adhere to the substrate via a potential,  $E_{adh.} = \frac{1}{2} \gamma \sum_i d_i^2 A_i$ , where  $d_i$  is the shortest Euclidean distance between the vertex  $i$  and the adhering surface.

The surface mesh with  $\approx 2 \times 10^4$  triangles was generated by constructing a Delaunay triangulation [26] of  $\approx 10^4$  randomly but evenly distributed points on a disk of radius  $R \approx 100a_0$ , where  $a_0$  is the average distance between two neighboring points. The initial state for each simulation was constructed by deforming the planar mesh to perfectly comply with a prescribed shape of the substrate, modeled as a hyperbolic paraboloid and

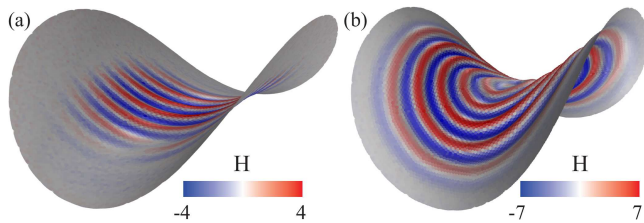


FIG. 4. (color online) Snapshots of the relaxed conformation of a sheet adhered to a negative curvature substrate modeled as a hyperbolic paraboloid surface,  $z(x, y) = \alpha x^2 - \beta y^2$ . For a substrate with a highly anisotropic shape ( $\alpha = 0.1a_0^{-1}$ ,  $\beta = 0.5a_0^{-1}$ ) one observes folds (a); sheets adhered to an isotropic substrate ( $\alpha = \beta = 0.5a_0^{-1}$ ) develop wrinkles (b). Mean curvature,  $H$ , is measured in units of  $a_0^{-1}$ .

parametrized as  $z(x, y) = \alpha x^2 - \beta y^2$ . A deformation pattern typically emerged within the first  $5 \cdot 10^4$  MC sweeps and was further relaxed for an additional  $2.5 \times 10^5$  sweeps. In all simulations the energy scale is set by the bending rigidity  $\kappa$  and we set  $Y = 10^3 \kappa / a_0^2$  (corresponding to the thickness  $t \approx 0.03a_0$ ),  $\gamma = 10\kappa / a_0^2$ , and  $\nu = 1/3$ .

In Fig. 3 we show a phase diagram of the wrinkle and fold patterns for  $\alpha, \beta \in [0, \dots, 0.5]$ , measured in units of  $a_0^{-1}$ . We note that the Gaussian curvature of a hyperbolic paraboloid surface is  $K_G(x, y) = -4\alpha\beta / (1 + 4x^2\alpha^2 + 4y^2\beta^2)^2$  and has a maximally negative  $K_G^{max} = -4\alpha\beta$  at  $x = y = 0$ . For small values of  $\alpha, \beta \lesssim 0.2a_0^{-1}$  the Gaussian curvature is very small,  $|K_G| \lesssim 0.15a_0^{-2}$  and the strong adhesion forces prevent the sheet from deforming; instead it remains smooth and perfectly compliant to the substrate. As  $\alpha$  and  $\beta$  increase two distinct deformed states form, folds and wrinkles. These can be distinguished by the isometry condition as follows. The inextensibility of a sheet sets an upper limit  $2R$ , the diameter of the planar sheet, as the maximal geodesic distance between two arbitrary points on a sheet contour. If the determined sheet contour has the maximum geodesic diameter equal to (smaller than)

$2R$ , then the sheet is recognized as having folds (wrinkles). An isotropic Gaussian curvature ( $\alpha = \beta$ , since  $K_G = f(\alpha^2 x^2 + \beta^2 y^2)$  [12]) imposes either isotropic tangential stretching or isotropic radial compression on the sheet, which is expected to result in wrinkles. As the Gaussian curvature grows increasingly anisotropic (the ratio  $\alpha/\beta$  deviates from unity), the imposed anisotropic stretching and compression on the sheet are expected to generate folds which are themselves anisotropic objects. This shows that wrinkles occur near the isotropic region while folds arise in the highly anisotropic regions. A typical configuration with folds is shown in Fig. 4a, while a typical wrinkle pattern is shown in Fig. 4b. Finally, in the highly anisotropic case,  $\alpha \ll \beta$ ,  $K_G \approx 0$  and the substrate is nearly cylindrical; in this case the deformation of the sheet is nearly isometric and no wrinkles or folds form.

In conclusion, using geometric arguments and numerical simulations of a thin-sheet elastic model we study the curvature-driven wrinkle/fold patterns of a flat sheet adhered to a negative curvature substrate. We analyze two types of structure, concentric wrinkles and eye-like folds, that are compatible with negative curvature liquid substrates and discuss the transition between these two states driven by the anisotropy of the background geometry. The ability of wrinkles/folds to deform a plane to a curved surface may find potential applications. Consider a flat sheet with a pre-designed wrinkle/fold pattern like the lines on a palm. By controlling the on/off status of the wrinkles/folds, a planar sheet can be programmed to buckle to a desired shape. This may lead to potential applications in maximizing sunshine harvest by designing the shape of ultra thin flexible solar cells [27]. Our study also sheds light on the reverse problem of attaching a curved shell to a flat substrate, e.g., the adhesion of a cell on a flat substrate [28].

We thank Jennifer Schwarz for kindly allowing us to use her computer resources. This work was supported by the National Science Foundation grant DMR-0808812 and by funds from Syracuse University.

\* Present address: Department of Materials Science and Engineering, Northwestern University, Evanston, Illinois, 60208-3108, USA

† e-mail: bowick@phy.syr.edu

- [1] J. Sadoc and R. Mosseri, *Geometrical Frustration* (Cambridge University Press, 2006).
- [2] E. Demaine, M. Demaine, J. Iacono, and S. Langerman, *Computational Geometry* **42**, 748 (2009).
- [3] J. Hure, B. Roman, and J. Bico, *Phys. Rev. Lett.* **106**, 174301 (2011).
- [4] T. Witten, *Rev. Mod. Phys.* **79**, 643 (2007).
- [5] H. King, R. Schroll, B. Davidovitch, and N. Menon, *Proc. Natl. Acad. Sci. U.S.A.* **109**, 9716 (2012).
- [6] B. Roman and J. Bico, *Journal of Physics: Condensed Matter* **22**, 493101 (2010).
- [7] M. Marder, E. Sharon, and R. D. Deegan, *Physics Today*

**60**, 33 (2007).

- [8] H. M. Winkler, *Bauhaus: Weimar, Dessau, Berlin, Chicago* (The MIT Press, 1978).
- [9] P. Jackson, *The Complete Origami Course* (Gallery Books, 1989).
- [10] J. Kim, J. Hanna, M. Byun, C. Santangelo, and R. Hayward, *Science* **335**, 1201 (2012).
- [11] B. Audoly and Y. Pomeau, *Elasticity and Geometry* (Oxford University Press, Oxford and New York, 2010).
- [12] D. Struik, *Lectures on Classical Differential Geometry* (Dover Publications, 1988).
- [13] P. Shipman and A. Newell, *Phys. Rev. Lett.* **92**, 168102 (2004).
- [14] K. Kasahara, *Extreme Origami* (Sterling Pub Co Inc, 2003).
- [15] H. Diamant and T. Witten, *Phys. Rev. Lett.* **107**, 164302

- (2011).
- [16] M. Bowick and L. Giomi, *Adv. Phys.* **58**, 449 (2009).
- [17] S. Houliara and S. Karamanos, *Int. J. Solids Struct.* **47**, 10 (2010).
- [18] E. Schmidt, *Mathematische Zeitschrift* **44**, 689 (1939).
- [19] W. Koiter, *Koninklijke Nederlandse Akademie van Wetenschappen, Proceedings, Series B* **69**, 1 (1966).
- [20] M. Do Carmo, *Differential Geometry of Curves and Surfaces*, vol. 1 (Prentice-Hall Englewood Cliffs, NJ, 1976).
- [21] M. Parrinello and A. Rahman, *J. Appl. Phys.* **52**, 7182 (1981).
- [22] R. Sknepnek and M. Olvera de la Cruz, *Phys. Rev. E* **85**, 050501(R) (2012).
- [23] K. Brakke, *The Motion of A Surface by Its Mean Curvature* (Princeton University Press Princeton, New Jersey, 1978).
- [24] K. Brakke, *Experimental Mathematics* **1**, 141 (1992).
- [25] A. Siber, *Phys. Rev. E* **73**, 061915 (2006).
- [26] CGAL, *Computational Geometry Algorithms Library*, <http://www.cgal.org>.
- [27] M. Kaltenbrunner, M. White, E. Glowacki, T. Sekitani, T. Someya, N. Sariciftci, and S. Bauer, *Nature Communications* **3**, 770 (2012).
- [28] E. Sackmann and R. Bruinsma, *ChemPhysChem* **3**, 262 (2002).